Fermi National Accelerator Laboratory

FERMILAB-Conf-90/32-E
[E-741/CDF]

The Dijet Invariant Mass at the Tevatron Collider*

The CDF Collaboration

presented by

Mauro Dell'Orso
Università di Pisa
Pisa, Italy

January 1990

* Published in the proceedings of the 8th Topical Workshop on $p\bar{p}$ Collider Physics, Castiglione della Pescaia, Italy, September 1-5, 1989.

CDF/PUB/JET/PUBLIC/1103
January 1990

THE DIJET INVARIANT MASS AT THE TEVATRON COLLIDER

CDF Collaboration*
Presented by Mauro Dell'Orso
Dipartimento di Fisica, Università di Pisa
Pisa, ITALY

The differential cross section as a function of the dijet invariant mass has been measured in 1.8 TeV ppbar collisions. A comparison to leading order QCD predictions is presented as well as a study of the sensitivity of the mass spectrum to the gluon radiation. The need to take radiation into account requires the study of its spatial distribution and the comparison of the data to the predictions of shower Monte Carlo programs like Isajet and Herwig.

1. INTRODUCTION

We measured the differential cross section of the process p + pbar → jet + jet + X as a function of the dijet invariant mass. The measurement was performed with the CDF detector[1] at a center of mass energy of 1.8 TeV at the Tevatron Collider in Fermilab. The present analysis is based on the sample of events collected in the 1988/89 run, amounting to a total integrated luminosity of 4.65 pb^{-1}.

The interest for such a measurement comes from different points of view.

a) It constitutes an important check of the QCD theoretical predictions and a probe for the possible internal structure of the quarks[2].
b) New and unexpected physics can show up as resonance bumps in the mass spectrum or, for negative results, limits can be defined on the mass of new particles as in the case of the axigluon[3].
c) A detailed study of the dependence of the mass spectrum on the number of jets helps in the difficult issue of analyzing the characteristics of gluon radiation in the parton-parton scattering process.

2. THE DIJET MASS SPECTRUM

2.1 Trigger

The events used in the analysis come from the JET_20, JET_40, and JET_60 online triggers. These triggers basically require the presence of at least one energy cluster in the calorimeter with a transverse energy greater than, respectively, 20, 40, and 60 GeV.

---

* see Appendix

Pub. Proceedings 8th Topical Workshop on Proton-Antiproton Collider Physics, Castiglione, Italy, September 1-5, 1989.

2.2 Clustering Algorithm

The clustering algorithm[4], which exploits the projective tower geometry of the CDF calorimeter, produces a list of energy clusters. It uses the following parameters:

- Cone radius $R = (\Delta\varphi^2 + \Delta\eta^2)^{1/2} = 0.7$ (the radius of the region where the calorimeter energy is integrated).
- Tower threshold $E_{thr} = 0.2$ GeV (the energy threshold for a calorimeter tower to enter the cluster energy sum).
- Seed tower threshold $E_{seed} = 1$ GeV (the threshold for a tower to initiate the cluster search).

The algorithm also gives the momentum of each cluster, assuming a massless particle for each calorimeter tower belonging to the cluster.

2.3 Energy Scale

The jet energy can be obtained from the cluster energy through an appropriate correction factor. CDF has a complete set of pseudorapidity dependent correction factors, obtained by a detailed study of p-pbar data, test beam data and Monte Carlo simulations[5].

For this analysis the jet energy (momentum) is defined as the total energy (momentum) of all the particles (leptons, mesons and baryons) exiting the primary vertex within a cone of fixed radius R = 0.7. As an example, although both charged tracks in fig. 1 hit the calorimeter outside the jet cone, the solid track is included in the jet definition while the dashed one is not. The correction factor takes into account the detector effects only, like the calorimeter response and the magnetic bending of the charged tracks.

It should be pointed out that no attempt is made to reconstruct the energy of the parton from which the jet originates. This "instrumental" jet definition is less model dependent than others and hopefully makes comparison of measurement with theoretical prediction less difficult, especially for higher order QCD calculations.

2.4 Event Selection

The criteria for the event selection are listed below.

a) $|Z_{vertex}| < 60$ cm; the longitudinal coordinate of the primary vertex was required to be within 60 cm of the center of the detector. This fiducial cut keeps the events inside the geometrical acceptance of the detector.

b) $|\Delta\varphi| < 20°$; the two leading jets where required to be back to back within 20° in the

transverse plane. This is a loose cut to select two jet events.

c) $| Y_{boost} | < 0.4$, $| Y^* | < 0.4$; the cross section was integrated over this rapidity region where $Y_{boost} = (Y_1 + Y_2) / 2$ is the rapidity of the center of mass of the two leading jets and $Y^* = (Y_1 - Y_2) / 2$ is the rapidity of the first jet in the center of mass frame. This cut also implies that both jets are measured by the central calorimeter.

2.5 Results

The invariant mass was calculated as $M_{jj} = [(E_1+E_2)^2 - (\mathbf{P}_1+\mathbf{P}_2)^2]^{1/2}$, where E_i and P_i are the measured energies and momenta of the two leading jets. Fig. 2 shows the plot of the differential cross section $d\sigma/dM_{jj}$ as a function of the dijet invariant mass M_{jj}. The dots represent the experimental points with their statistical errors. It should be noted that the measurement extends over a range of nearly 6 orders of magnitude.

The two solid lines across the plot define a band of uncertainty in the theoretical prediction (see below).

The relative systematic error on the cross section is roughly constant with the mass and smaller than 30%. Fig. 3 shows a breakdown of the systematic error into the main contributions[6] as a function of the invariant mass.

The smearing effect on the data points due to the finite resolution of the M_{jj} measurement has been taken into account and fig. 2 shows the points after the unsmearing correction[7]. Because of the low statistics at high masses the plot has been rebinned into larger bins for Mjj > 400 GeV. The data before the unsmearing and the rebinning are shown in fig. 4 for reference.

3. COMPARISON WITH THEORY

3.1 QCD Leading Order

To obtain the theoretical band in fig. 2 we calculated the predictions for the $2 \rightarrow 2$ QCD diagrams, varying the Q^2 within the range $0.5\ P_t^2 < Q^2 < 2\ P_t^2$ and using different parametrizations for the structure functions, namely EHLQ1, DO1, DO2, GHR[2,8,9]. The band in fig. 2 is the envelope of all the predictions for different Q^2 and structure functions.

It should be noted that these QCD predictions refer to the leading order QCD matrix element and do not take into account gluon radiation from the initial and final state partons.

3.2 Compositeness

To get a feeling for the sensitivity of the mass spectrum to the compositeness of the quarks, we superimposed the data onto the predictions obtained adding an effective 4-quark contact interaction[2] to the standard QCD lagrangian. Fig. 5 shows the prediction for different values of the compositeness energy Λ^*; as $\Lambda^* \to \infty$ the prediction approaches the pure QCD calculation. At energies less than the compositeness scale, a possible structure should show up as an increase of cross section at high masses.

The comparison with the data is done on an absolute scale without relative normalization between data and theoretical curve. Moreover the curve is calculated at fixed $Q^2 = P_t^2$ and for only one structure function, namely EHLQ1. A more detailed compositeness analysis will require normalizing the theoretical curve to the data at lower masses as well as varying the Q^2 and the structure functions. This analysis is in our plans for the near future.

4. QCD RADIATION

4.1 Effect of Radiation

As we said, a direct comparison of the measured mass spectrum with the $2 \to 2$ QCD calculations does not include the possibility of gluon radiation which generates secondary jets.

To measure the effect of the radiation on the cross section we added the non-leading jets in the computation of the invariant mass, whenever the distance (in η-φ space) from one of the leading jets was smaller than a fixed radius R_{cut}. The cut is intended to reject the jets generated by initial state radiation, which are likely to be away from the directions of the final state partons. We then looked at the dependence of the mass spectrum on the value of R_{cut}.

Fig. 6 shows how the cross section changes as R_{cut} changes. The dependence on R_{cut} is shown more clearly on the linear scales of fig. 7. This figure shows, for different values of the sum cone radius R_{cut}, the ratio of the mass spectrum with the jet merging to the mass spectrum of the two leading jets. The effect grows up to a factor 2 for a radius $R_{cut} = 1.6$.

4.2 Distribution of Radiation

To understand where the non-leading jets responsible for the increase of the cross section in fig. 6-7 come from, we plotted the position of the third jet with respect to the

leading jets (the jets are numbered with decreasing transverse energy order). In the scatter plot of fig. 8 each point refers to the position of the third jet in one event. The horizontal axis represents the φ distance between the third jet and the second jet, while the vertical axis represents the η distance. The second jet in the scatter plot is at the origin.

Much energy is clustered near the second jet; the probability for the energy to come from the final state is higher when approaching the leading clusters, while the initial state bremsstrahlung is expected to be less correlated with them. To further investigate the dynamical information contained in the scatter plot of fig. 8. we looked for some suitable variables which could exhibit dynamical properties.

We will see in the next paragraph an example of such a variable. but it is worth underlining here that the influence of the gluon radiation requires the use of shower Monte Carlo programs, like for example Isajet[10], as tools for comparing data with theory. These Monte Carlos provide a way for handling the radiation which is complementary to the higher order QCD calculations. Because of the relevance of the radiation and its simulation, we are testing and comparing the data with the predictions from two of the more widely used shower Monte Carlo programs: Isajet and Herwig[11].

4.3 Comparing Isajet and Herwig

One interesting characteristic of the radiation, that allows a direct comparison between different Monte Carlos, is its spatial distribution around the second jet. The distribution has been studied as described in the following.

a) We took the scatter plot in fig. 8, which represents the density $\rho(\Delta\varphi, \Delta\eta)$ of the third jet in the space around the second jet.
b) We changed the coordinates from the "cartesian" $\Delta\varphi$, $\Delta\eta$ to the "polar" R, α (see fig. 8 for a clear definition of R and α) and we defined the density as a function of the new coordinates $\sigma(R, \alpha) = \rho(\Delta\varphi, \Delta\eta)$.
c) We divided the scatter plot into a number of slices, each slice having a fixed value of the "polar" angle α.
d) We studied the α dependence of the third jet distribution σ, integrating the density on each slice over the range $1.5 < R < 3.14$: $\int\sigma(R, \alpha)RdR$.

Fig. 9 shows the density of the third jet, integrated over R, as a function of α. This plot shows an enhancement of the density at $\alpha \approx 90°$. For comparison we simulated events using the Isajet and Herwig Monte Carlos together with the CDF detector simulator QFL[12], and we applied the same analysis program to the simulated events as

we applied to the real data. The plots so obtained are shown in fig. 10. As it turns out from this figure, Isajet does not reproduce the enhancement at high α, while Herwig does a better job.

Looking back to fig. 8, it turns out that $\alpha \approx 90°$ means small $\Delta\varphi$ and small distance from the plane defined by the second jet and the beam axis (which is the plane identified by $\Delta\varphi = 0$). This suggests that the enhancement may come from an effect of interference between coherent colored radiation from the initial and the final partons[11]. If this is the case, the difference between Isajet and Herwig is easily explained by the different way the two programs deal with the radiation: incoherently the first and coherently the second.

At any rate much work remains to be done on the subject of QCD radiation and comparison between shower Monte Carlos, before having enough confidence on the detailed verification of theoretical predictions.

5. CONCLUSIONS

a) We measured the differential cross section $d\sigma/dM_{jj}$ as a function of the invariant mass M_{jj}.

b) A first comparison to the theoretical prediction from $2 \rightarrow 2$ QCD calculations is OK, and further analysis is under way to give a quantitative limit for quark compositeness.

c) The mass spectrum is more exclusive than the E_t spectrum and it is more sensitive to the details of the QCD radiation, allowing a deeper probing of theoretical predictions.

d) The spatial distribution of the 3rd jet shows a discrepancy from the Isajet prediction and it is in better agreement with Herwig.

e) We have in progress detailed tests on possible structures in the mass spectrum to give limits on the axigluon mass and to search for bumps, using cuts that enhance the jet energy resolution.

REFERENCES

1) F. Abe et al., Nucl. Instr. and Meth. **A271** (1988) 387
2) E. Eichten et al., Rev. Mod. Phys. **56** (1984) 579
3) P.H. Frampton and S.L. Glashow, Phys. Lett. **B190** (1987) 157
4) D. Brown et al., CDF Internal Note **605** (1988)
5) D. Brown and R. Carey, CDF Internal Note **755** (1988)
6) M. Dell'Orso et al., CDF Internal Note **1057** (1989)
7) M. Dell'Orso et al., CDF Internal Note **1056** (1989)
8) D. Duke and J. Owens, Phys. Rev. **D30** (1984) 49
9) M. Glueck et al., Z. Phys. **C13** (1982) 119
10) F.E. Paige and S.D. Protopopescu, Brookhaven National Lab. Report **37066** (1985)
11) G. Marchesini and B. Webber, Nucl. Phys. **B310** (1988) 461
12) D. Brown et al., CDF Internal Note **753** (1988)

Appendix: The CDF Collaboration.

F. Abe,[8] D. Amidei,[4] G. Apollinari,[11] M. Atac,[4] P. Auchincloss,[14] A. R. Baden,[6] A. Bamberger,[19] A. Barbaro-Galtieri,[9] V. E. Barnes,[12] F. Bedeschi,[11] S. Behrends,[2] S. Belforte,[11] G. Bellettini,[11] J. Bellinger,[18] J. Bensinger,[2] A. Beretvas,[4] J. P. Berge,[4] S. Bertolucci,[5] S. Bhadra,[7] M. Binkley,[4] R. Blair,[1] C. Blocker,[2] A. W. Booth,[4] G. Brandenburg,[6] D. Brown,[6] E. Buckley,[14] A. Byon,[12] K. L. Byrum,[18] C. Campagnari,[3] M. Campbell,[3] R. Carey,[6] W. Carithers,[9] D. Carlsmith,[18] J. T. Carroll,[4] R. Cashmore,[19] F. Cerveili,[11] K. Chadwick,[4] G. Chiarelli,[5] W. Chinowsky,[9] S. Cihangir,[4] A. G. Clark,[4] D. Connor,[10] M. Contreras,[2] J. Cooper,[4] M. Cordelli,[5] D. Crane,[4] M. Curatolo,[5] C. Day,[4] S. Dell'Agnello,[11] M. Dell'Orso,[11] L. Demortier,[2] P. F. Derwent,[3] T. Devlin,[14] D. DiBitonto,[15] R. B. Drucker,[9] J. E. Elias,[4] R. Ely,[9] S. Errede,[7] B. Esposito,[5] B. Flaugher,[14] G. W. Foster,[4] M. Franklin,[6] J. Freeman,[4] H. Frisch,[3] Y. Fukui,[8] Y. Funayama,[16] A. F. Garfinkel,[12] A. Gauthier,[7] S. Geer,[6] P. Giannetti,[11] N. Giokaris,[13] P. Giromini,[5] L. Gladney,[10] M. Gold,[9] K. Goulianos,[13] H. Grassmann,[11] C. Grosso-Pilcher,[3] C. Haber,[9] S. R. Hahn,[4] R. Handler,[18] K. Hara,[16] R. M. Harris,[9] J. Hauser,[3] T. Hessing,[15] R. Hollebeek,[10] L. Holloway,[7] P. Hu,[14] B. Hubbard,[9] B. T. Huffman,[12] R. Hughes,[10] P. Hurst,[7] J. Huth,[4] M. Incagli,[11] T. Ino,[16] H. Iso,[16] H. Jensen,[4] C. P. Jessop,[6] R. P. Johnson,[4] U. Joshi,[4] R. W. Kadel,[4] T. Kamon,[15] S. Kanda,[16] D. A. Kardelis,[7] I. Karliner,[7] E. Kearns,[6] R. Kephart,[4] P. Kesten,[2] R. M. Keup,[7] H. Keutelian,[7] S. Kim,[16] L. Kirsch,[2] K. Kondo,[16] S. E. Kuhlmann,[1] E. Kuns,[14] A. T. Laasanen,[12] J. I. Lamoureux,[18] W. Li,[1] T. M. Liss,[7] N. Lockyer,[10] C. B. Luchini,[7] P. Maas,[4] M. Mangano[11] J. P. Marriner,[4] R. Markeloff,[18] L. A. Markosky,[18] R. Mattingly,[2] P. McIntyre,[15] A. Menzione,[11] T. Meyer,[15] S. Mikamo,[8] M. Miller,[3] T. Mimashi,[16] S. Miscetti,[5] M. Mishina,[8] S. Miyashita,[16] Y. Morita,[16] S. Moulding,[2] A. Mukherjee,[4] L. F. Nakae,[2] I. Nakano,[16] C. Nelson,[4] C. Newman-Holmes,[4] J. S. T. Ng,[6] M. Ninomiya,[16] L. Nodulman,[1] S. Ogawa,[16] R. Paoletti,[11] A. Para,[4] E. Pare,[6] J. Patrick,[4] T. J. Phillips,[6] R. Plunkett,[4] L. Pondrom,[18] J. Proudfoot,[1] G. Punzi,[11] D. Quarrie,[4] K. Ragan,[10] G. Redlinger,[3] J. Rhoades,[18] M. Roach,[17] F. Rimondi,[19] L. Ristori,[11] T. Rohaly,[10] A. Roodman,[3] A. Sansoni,[5] R. D. Sard,[7] A. Savoy-Navarro,[19] V. Scarpine,[7] P. Schlabach,[7] E. E. Schmidt,[4] M. H. Schub,[12] R. Schwitters,[6] A. Scribano,[11] S. Segler,[4] Y. Seiya,[16] M. Sekiguchi,[16] P. Sestini,[11] M. Shapiro,[6] M. Sheaff,[18] M. Shochet,[3] J. Siegrist,[9] P. Sinervo,[10] J. Skarha,[18] K. Sliwa,[17] D. A. Smith,[11] F. D. Snider,[3] R. St. Denis,[6] A. Stefanini,[11] R. L. Swartz, Jr.,[7] M. Takano,[16] K. Takikawa,[16] S. Tarem,[2] D. Theriot,[4] M. Timko,[15] P. Tipton,[9] S. Tkaczyk,[4] A. Tollestrup,[4] G. Tonelli,[11] J. Tonnison,[12] W. Trischuk,[6] Y. Tsay,[3] F. Ukegawa,[16] D. Underwood,[1] R. Vidal,[4] R. G. Wagner,[1] R. L. Wagner,[4] J. Walsh,[10] T. Watts,[14] R. Webb,[15] C. Wendt,[18] W. C. Wester, III,[9] T. Westhusing,[11] S. N. White,[13] A. B. Wicklund,[1] H. H. Williams,[10] B. Winer,[9] A. Yagil,[4] A. Yamashita,[16] K. Yasuoka,[16] G. P. Yeh,[4] J. Yoh,[4] M. Yokoyama,[16] J. C. Yun,[4] **F. Zetti**[11]

[1] *Argonne National Laboratory, Argonne, Illinois 60439*

[2] *Brandeis University, Waltham, Massachusetts 02254*

[3] *University of Chicago, Chicago, Illinois 60637*

[4] *Fermi National Accelerator Laboratory, Batavia, Illinois 60510*

[5] *Laboratori Nazionali di Frascati, Istituto Nazionale di Fisica Nucleare, Frascati, Italy*

[6] *Harvard University, Cambridge, Massachusetts 02138*

[7] *University of Illinois, Urbana, Illinois 61801*

[8] *National Laboratory for High Energy Physics (KEK), Tsukuba-gun, Ibaraki-ken 305, Japan*

[9] *Lawrence Berkeley Laboratory, Berkeley, California 94720*

[10] *University of Pennsylvania, Philadelphia, Pennsylvania 19104*

[11] *Istituto Nazionale di Fisica Nucleare, University and Scuola Normale Superiore of Pisa, I-56100 Pisa, Italy*

[12] *Purdue University, West Lafayette, Indiana 47907*

[13] *Rockefeller University, New York, New York 10021*

[14] *Rutgers University, Piscataway, New Jersey 08854*

[15] *Texas A&M University, College Station, Texas 77843*

[16] *University of Tsukuba, Ibaraki 305, Japan*

[17] *Tufts University, Medford, Massachusetts 02155*

[18] *University of Wisconsin, Madison, Wisconsin 53706*

[19] *Fermilab Visiting Physicist*

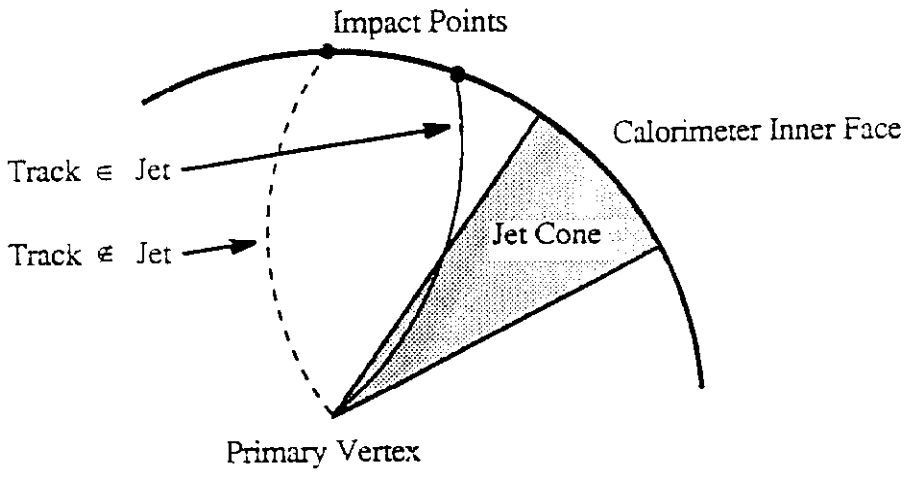

FIG. 1: JET DEFINITION

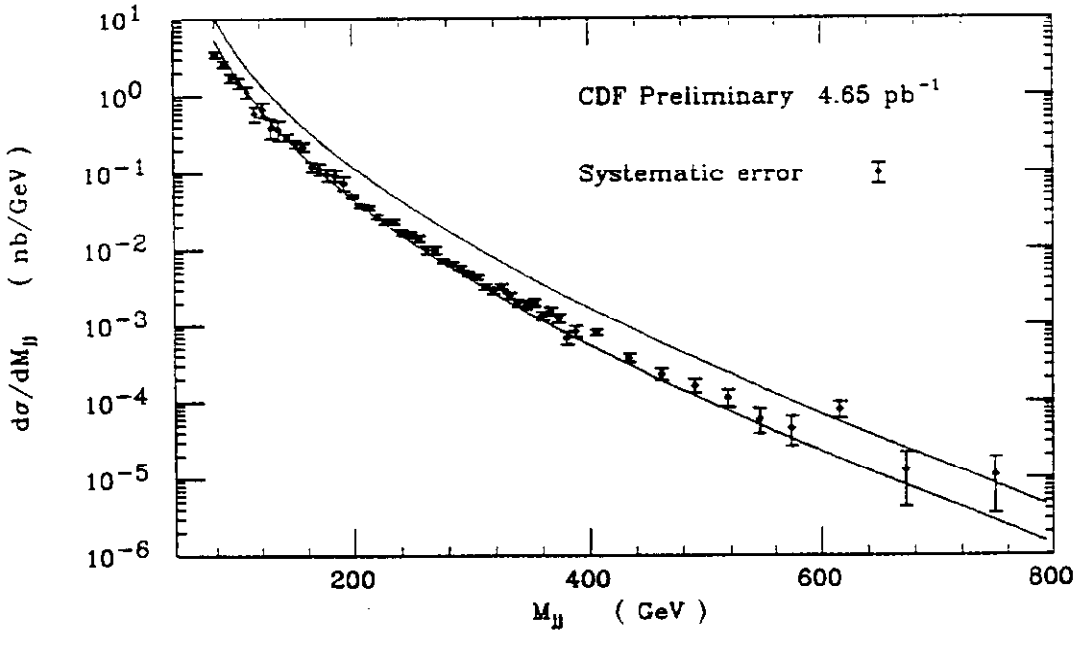

FIG. 2: DI-JET MASS SPECTRUM

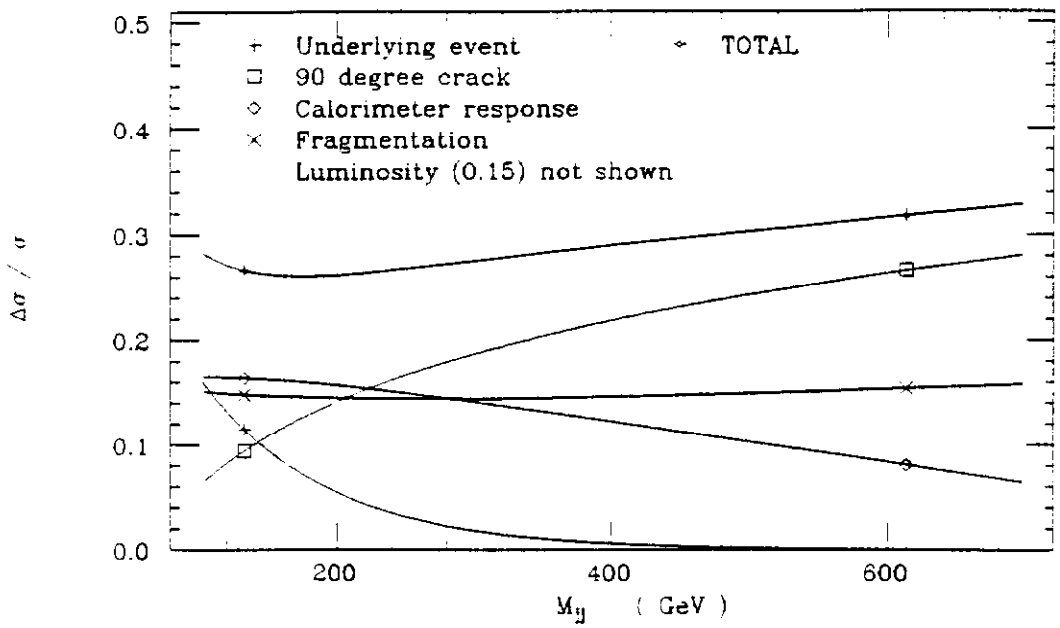

FIG. 3: SYSTEMATICS

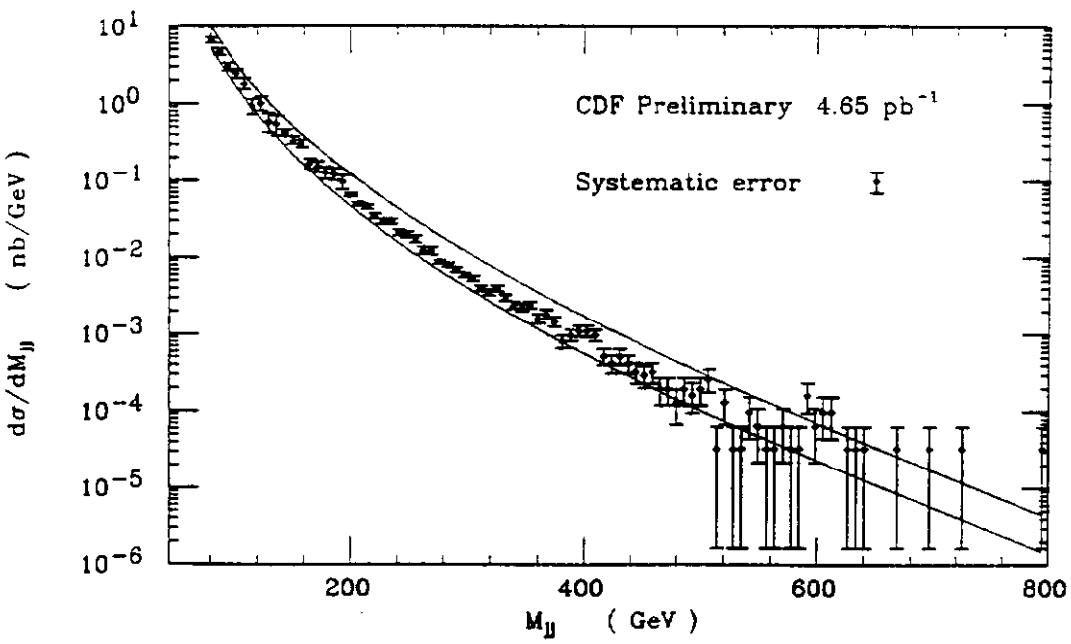

FIG. 4: MASS SPECTRUM BEFORE UNSMEARING AND REBINNIG

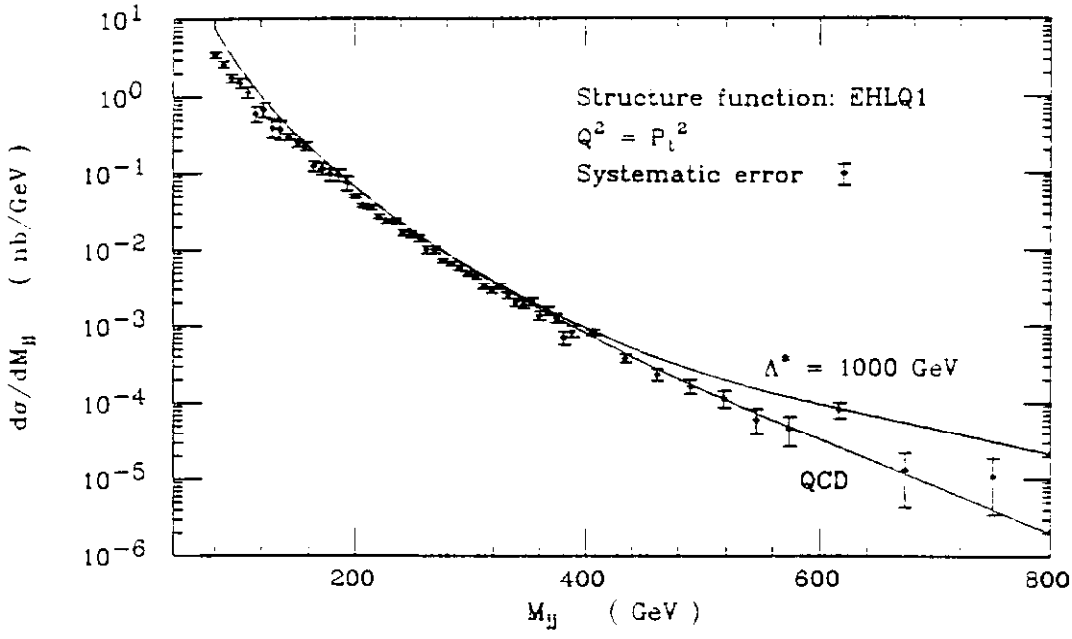

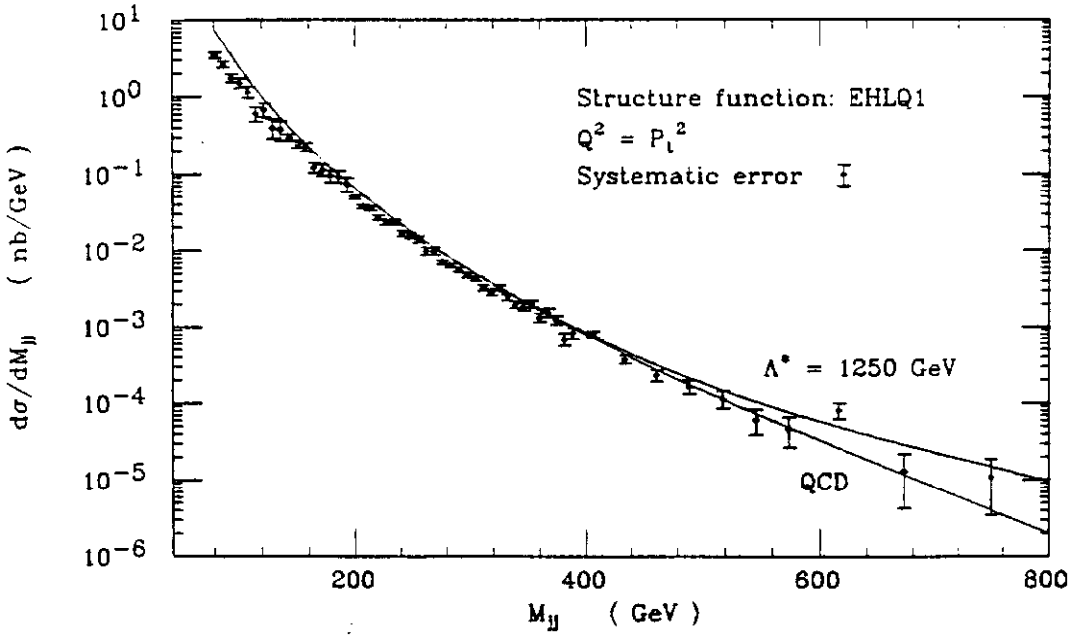

FIG. 5: PREDICTIONS FOR COMPOSITENESS SCALE Λ^*

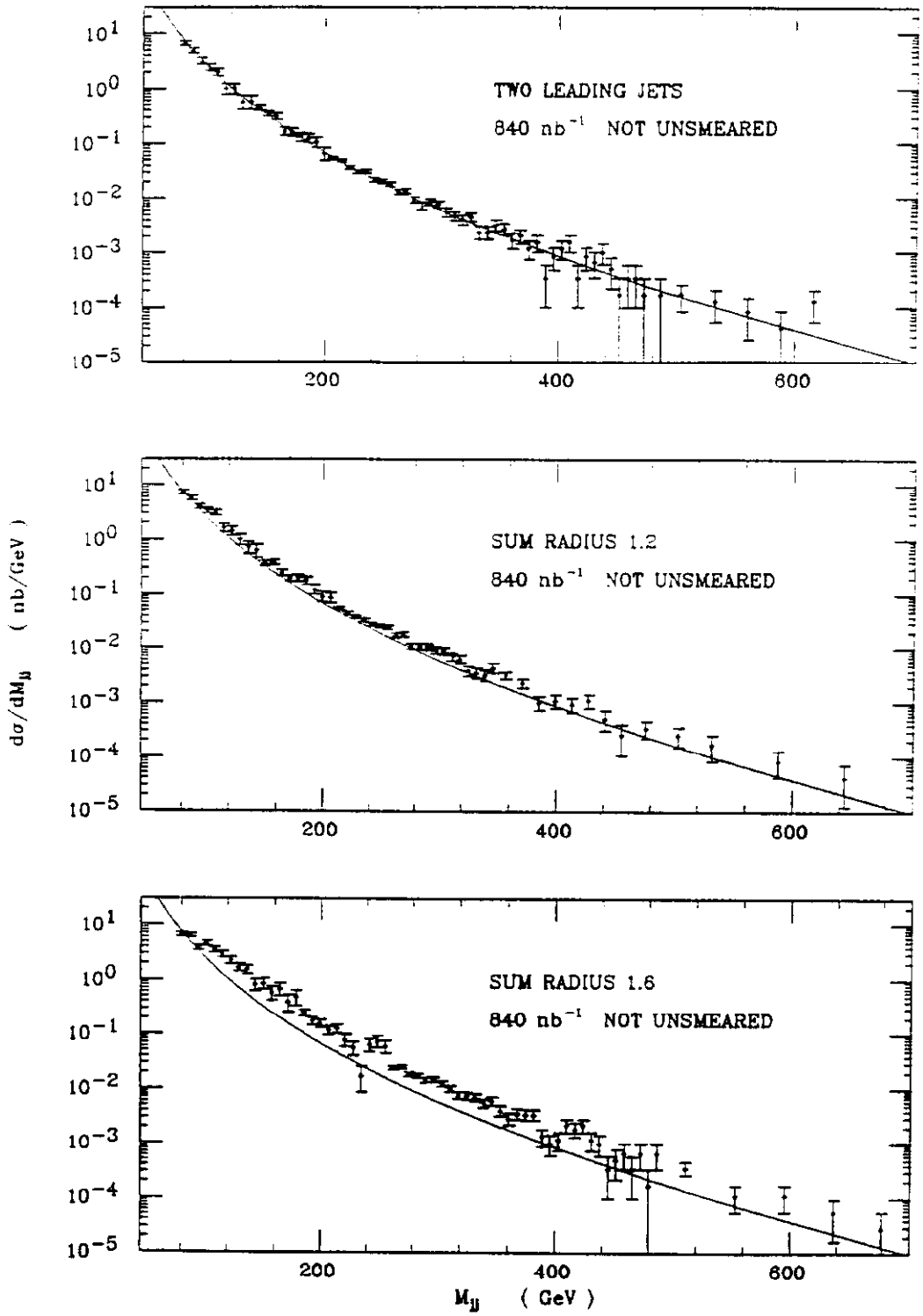

FIG. 6: DEPENDENCE OF MASS SPECTRUM ON THE SUM CONE RADIUS

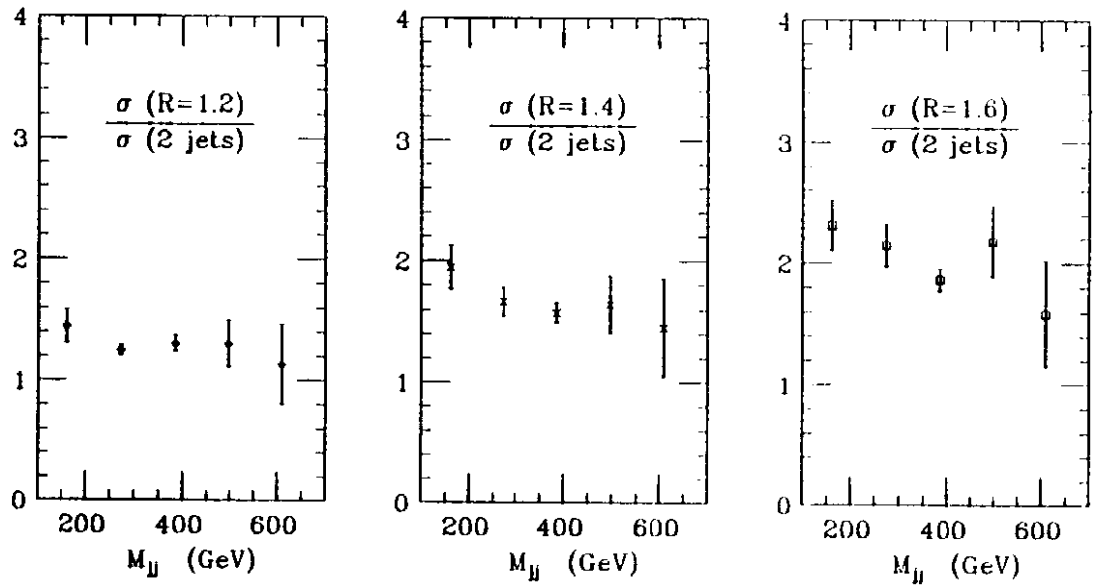

FIG. 7: SPECTRUM AFTER MERGING OVER SPECTRUM BEFORE MERGING

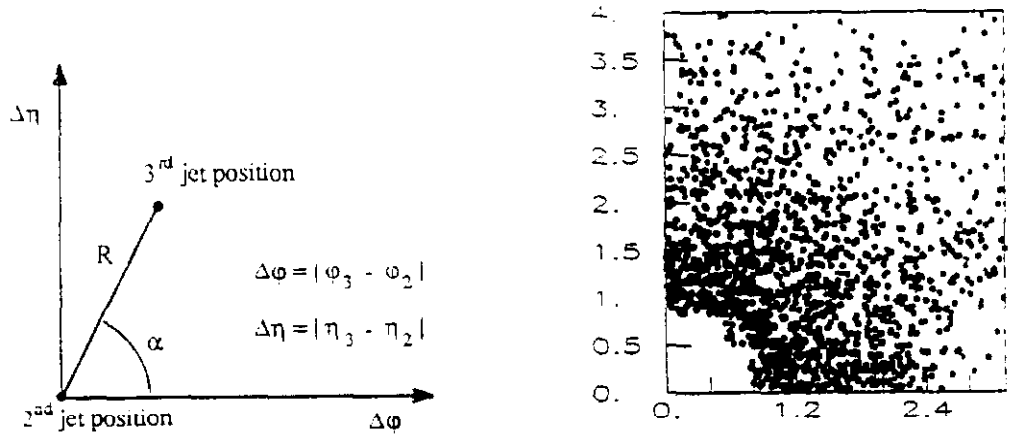

FIG. 8: SPATIAL DISTRIBUTION OF THE THIRD JET

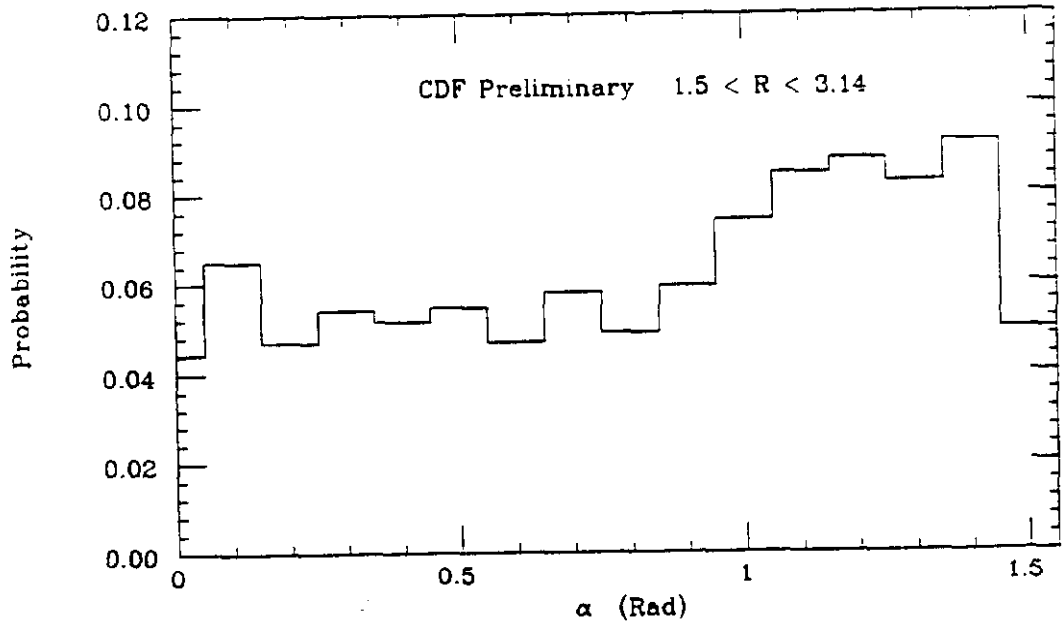

FIG 9: SPATIAL DISTRIBUTION OF THE 3rd JET AROUND THE 2nd JET, INTEGRATED OVER R (see text)

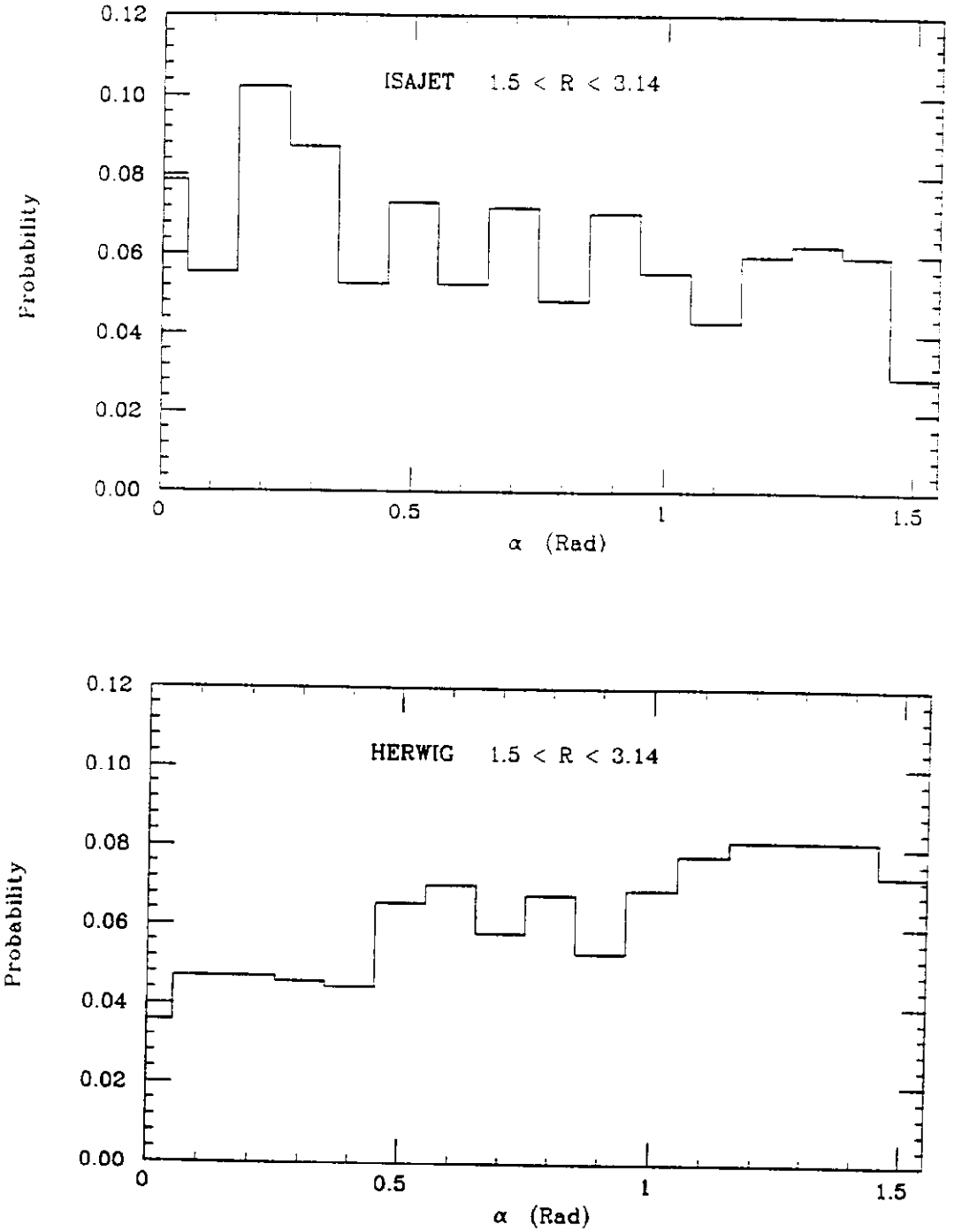

FIG 10: MONTECARLO PREDICTIONS FOR THE SPATIAL DISTRIBUTION OF THE 3rd JET AROUND THE 2nd JET (see text)